Phase behaviour of the symmetric binary mixture from thermodynamic perturbation theory

2010 J. Phys.: Condens. Matter 22 104113

(http://iopscience.iop.org/0953-8984/22/10/104113)

J. Phys.: Condens. Matter **22** (2010) 104113 (11pp) doi:10.1088/0953-8984/22/10/104113

Phase behaviour of the symmetric binary mixture from thermodynamic perturbation theory

N Dorsaz and G Foffi

Institute of Theoretical Physics and Institut Romand de Recherche Numérique en Physique des Matériaux (IRRMA), Ecole Polytechnique Fédérale de Lausanne (EPFL), 1015 Lausanne, Switzerland

E-mail: nicolas.dorsaz@a3.epfl.ch and giuseppe.foffi@epfl.ch

Received 1 October 2009, in final form 19 November 2009
Published 23 February 2010
Online at stacks.iop.org/JPhysCM/22/104113

Abstract

We study the phase behaviour of symmetric binary mixtures of hard core Yukawa (HCY) particles via thermodynamic perturbation theory (TPT). We show that all the topologies of phase diagram reported for the symmetric binary mixtures are correctly reproduced within the TPT approach. In a second step we use the capability of TPT to be straightforwardly extended to mixtures that are nonsymmetric in size. Starting from mixtures that belong to the different topologies of symmetric binary mixtures we investigate the effect on the phase behaviour when an asymmetry in the diameters of the two components is introduced. Interestingly, when the energy of interaction between unlike particles is weaker than the interaction between like particles, the propensity for the solution to demix is found to increase strongly with size asymmetry.

(Some figures in this article are in colour only in the electronic version)

1. Introduction

While the study of one component fluid phase diagrams is standard practice [1], the investigations of, even simple, binary mixtures phase diagrams are much more challenging due to the increase in the number of parameters [2–4]. As predicted by Gibbs rule, in addition to the liquid–vapour phase separation observed in one component systems, binary mixtures can also undergo a demixing transition. The phase diagram is thus determined by the competition between liquid–vapour and mixing–demixing phase separation. The presence of an additional degree of freedom, the concentration of the two species, considerably widens the spectrum of critical behaviours: tricritical points, critical end points, four phase points and critical lines replace the simple critical point and triple point found in one component fluids [3].

In order to reduce drastically the parameter space, in an attempt to study quantitatively the phase behaviour of binary mixtures, some works focused on the so-called symmetric binary mixtures. In this class of systems, the two components have the same diameters ($d_{11} = d_{22} = d_{12} = d$) and the attraction strengths between like particles are equal, while the ratio of the interaction strengths between unlike species δ is introduced as tunable parameter. The phase behaviour of symmetrical binary mixtures has been studied by means of liquid state theories and computer simulations, but these investigations have been mainly limited to the equimolar plane of the phase diagram ($x = 1/2$) [4–6], while relatively few studies of the more general case of non-equimolar concentrations can be found in the literature. From these studies, different topologies of phase behaviour emerge in agreement with the mean field predictions. In particular, the value of δ is the key parameter that lies at the origin of these different topologies.

Only recently, insights into the complexity of the entire phase diagram of symmetric binary mixtures have been obtained using the hierarchical reference theory (HRT) [3]. This accurate theory introduces long-range density and concentration fluctuations via a renormalization procedure, where the long wavelength Fourier components of the microscopic interaction are gradually introduced in the Hamiltonian of the mixture [7, 8].

A systematic investigation of the full phase diagram for one of the archetypes of the symmetric binary mixture phase diagram, based on the mean spherical approximation (MSA) and complemented with grand canonical Monte Carlo (GCMC) simulations, has also been recently presented [9]. In this case, even if MSA is less accurate than more advanced liquid state theories, particularly in the critical regions, semiquantitative agreement with the MC simulations was obtained. This work confirmed the results obtained previously via HRT and complemented it, since the full coexistence phase diagram was calculated.

One natural question to ask is what is the effect of an asymmetry in the interactions. In particular, it would be important to understand what features of the symmetric mixtures survives. Both HRT and MSA are possible tools to undertake such an investigation. HRT, however, is already very laborious and computationally expensive for the symmetric mixture. Moreover its generalization to nonsymmetric binary mixtures is not straightforward [10]. On the other hand, the convergency of the semi-analytical MSA is also not guaranteed when moving to asymmetric mixtures, especially for strong asymmetry.

To gain insights into the properties of liquid systems, thermodynamic perturbation theories (TPT) have been of great importance when there are reference systems that are fully tractable. Besides the great success in atomic and molecular liquids [1], TPT have had a great impact on colloidal systems. Probably, the most important result was obtained for monodisperse short-range fluids. In fact, Gast *et al* were able to describe the phase diagram of colloidal particles interacting by depletion interactions [11], proposing, for the first time, the existence of a metastable liquid–liquid coexistence line in short-range attractive colloidal systems. More recently, thermodynamic perturbation theory was used to understand the interplay between phase coexistence and the glass line [12]. If the perturbative approach is known to give quantitatively imprecise results near phase boundaries and near criticality, it can be quantitatively correct elsewhere and it is an invaluable tool to predict the main features of the thermodynamic phase diagrams in liquids. Moreover, the method can be applied to very general mixtures, for which the convergence of integral equations is still out of reach.

In this paper we will apply TPT to describe the phase behaviour of the symmetric mixtures. We shall show that the main topologies obtained from HRT, MSA or GCMC approaches [3, 5, 9] are recovered within perturbation theory. In a second step we will consider symmetric mixtures of Yukawa particles which belong to the different classes of phase diagram and introduce a slight asymmetry in the diameters of the two components. This size asymmetry, which suppresses some artificial topologies of the symmetric cases, leads to an interesting variety of phase diagrams that are, at the moment, very difficult to assess by theoretical or computational techniques. Indeed, TPT has been successfully applied to study binary mixtures of eye lens proteins [13]. In this highly asymmetric case, a qualitative, even quantitative in some cases, agreement with the simulations was obtained [14].

2. Thermodynamic perturbation theory

2.1. Helmholtz free energy

We study the phase diagram of binary fluid mixtures through a thermodynamic perturbative approach [1, 15]. The equation of state of the interacting system is derived by treating the attractive potential $u_{ij}(r)$ as a perturbation of the hard-sphere potential $u^0_{ij}(r)$. This leads to an expression for the Helmholtz free energy F in terms of the average of $\beta u(r)$ and its powers taken over the unperturbed binary hard-sphere fluid ensemble. This reads for the first-order case:

$$\frac{F - F_0}{Nk_BT} = \frac{1}{2}\rho\beta \sum_{i,j=1}^{2} x_i x_j \int u_{ij}(\mathbf{r}) g^0_{ij}(\mathbf{r})\, \mathrm{d}\mathbf{r} + O(\beta^2) \quad (1)$$

where F_0 and $g^0_{ij}(R)$ are the free energy and the partial radial distribution function of the unperturbed system. A binary mixture of spherical particles of radius d_1 and d_2 is unequivocally defined by giving the number of particles of each kind, N_i $(i = 1, 2)$, and the volume V occupied by the system. The overall number density is then defined by $\rho = (N_1 + N_2)/V$ and the mole fraction, which gives the relative concentration of the two species, by $x = N_1/N$. We used the Boublik–Mansoori–Carnahan–Starling–Leland (BMCSL) equation of state for the free energy of the binary hard-sphere reference mixture F_0 [16], and the partial radial distribution $g^0_{ij}(r)$ functions were computed solving the Ornstein–Zernike equations with the partial direct correlation functions $c_{ij}(r)$ of the binary mixture obtained by Lebowitz within the Percus–Yevick (PY) approximation [17]. To correct the shortcomings of the PY hard-sphere distribution functions we used the Grundke–Henderson procedure, a generalization to mixtures of the Verlet–Weis modifications [18, 19]. The thermodynamics obtained via the Grundke–Henderson procedure is consistent with the BMCSL equation of state. Details of the calculation of the hard-sphere reference mixture properties can be found in [14].

2.2. Stability criteria: the spinodal

It is convenient to scale F and the other extensive variables, V and N_i $(i = 1, 2)$, by the total number of particles $N = N_1 + N_2$. The reduced free energy $f = F/N$ is then a function of the volume per particle $v = \rho^{-1}$ and the mole fraction x, as in equation (1). The condition of thermodynamic stability of binary mixtures can be expressed in terms of the derivatives of the Helmholtz free energy per particle f [20]

$$f_{xx} > 0 \qquad \text{and} \qquad f_{vv} - \frac{f^2_{vx}}{f_{xx}} > 0 \quad (2)$$

$$f_{vv} > 0 \qquad \text{and} \qquad f_{xx} - \frac{f^2_{vx}}{f_{vv}} > 0 \quad (3)$$

where $f_{\mu\nu} \equiv \frac{1}{2}(\frac{\partial^2 f}{\partial\mu\partial\nu})_T$ and $f_{\mu\mu} \equiv \frac{1}{2}(\frac{\partial^2 f}{\partial\mu^2})_{T,\nu}$ $(\mu, \nu = v, x)$. In one component systems, the instability can be only driven by mechanical instability, i.e. by density fluctuations. For binary mixtures, besides mechanical instability, strong *concentration*

fluctuations can lead to material instability. The latter lead to demixing, i.e. a separation of the system into phases of different concentrations. Except in special cases, both mechanical and material instabilities will in general appear simultaneously [2].

2.3. Main fluctuations driving the instability

In order to determine to what degree the instability is driven by largest mechanical or material fluctuations (i.e. density or concentration fluctuations) it is useful to diagonalize the stability matrix $[f]$ (i.e. the matrix of the partial derivatives of f) through an orthogonal change of basis [20, 21]. The eigenvalues are given by:

$$\lambda_\pm = \tfrac{1}{2}\mathrm{tr}[f] \pm \tfrac{1}{2}\sqrt{\mathrm{tr}[f]^2 - 4\det[f]} \tag{4}$$

and the normalized eigenvectors can be written:

$$\mathbf{z}_\pm = \begin{pmatrix} x_\pm \\ y_\pm \end{pmatrix} \tag{5}$$

with:

$$x_\pm = 1\Big/\sqrt{1+\left[\frac{f_{vv}-\lambda_\pm}{f_{vx}}\right]^2} \qquad y_\pm = -x_\pm\frac{f_{vv}-\lambda_\pm}{f_{vx}}. \tag{6}$$

The nature of the instability can be characterized defining the angle α

$$\alpha = \arctan\left(\frac{x_-}{y_-}\right) \tag{7}$$

with the argument that simplifies to

$$\frac{x_-}{y_-} = -\frac{f_{vx}}{f_{vv}-\lambda_-}. \tag{8}$$

When an instability is reached, the stability matrix becomes singular and the determinant $\det[f] \equiv \lambda_-\lambda_+$ vanishes, a condition that is independent of the basis chosen to diagonalize the quadratic form. The border of a stability region is thus indicated by the smaller eigenvalue λ_- going to zero.

The above relation holds for $[f]$ nondiagonal ($f_{vx} \neq 0$). The angle α is the angle between the eigenvector corresponding to the smallest eigenvalue $\mathbf{z}_-$ and the axis representing the concentration fluctuations. If α is equal to zero, the eigenvector is aligned to it and pure concentration fluctuations dominate. On the other hand, if α is equal to $\pm\pi/2$, only density fluctuations are present in the system. These limiting situations are only encountered in special cases. In general, the instability will be predominantly of demixing type, when α is close to 0, and of condensation type, when α is close to $\pm\pi/2$.

This formalism was first introduced by Chen and Forstmann [21] to characterize the instability of binary mixtures as an alternative to the Bhatia–Thornton partial structure factors [22]. The latter, which can also be measured in principle in simulations, and whose divergence is a good indicator of instabilities of pure condensation or pure demixing, are less suited when fluctuations in both density and concentration are taking place at the same time.

2.4. Phase coexistence: the binodal

Within the TPT approach we do not have access directly to the coexisting (binodal) surface. In order to build the whole coexisting surface we have to pass through the determination of (all) the coexisting phases and related tie lines in the system. Two phases (I and II) coexist if the pressure and the chemical potential of each species (1 and 2) are equal in both phases, i.e:

$$P^{(\mathrm{I})} = P^{(\mathrm{II})}, \qquad T^{\mathrm{I}} = T^{\mathrm{II}} \qquad \mu_1^{(\mathrm{I})} = \mu_1^{(\mathrm{II})} \qquad \mu_2^{(\mathrm{I})} = \mu_2^{(\mathrm{II})}. \tag{9}$$

This is a non-linear system of equations that must be solved numerically. We use a Newton–Raphson algorithm to solve them and to compute the binodal.

2.5. Critical lines and critical end points (CEP)

At a critical point, the tie lines that join coexisting phases become tangent to the curve bounding the instable region [2]. This condition can be expressed as:

$$f_{xxx} - 3f_{xxv}\left(\frac{f_{xv}}{f_{vv}}\right) + 3f_{xvv}\left(\frac{f_{xv}}{f_{vv}}\right)^2 - f_{vvv}\left(\frac{f_{xv}}{f_{vv}}\right)^3 = 0. \tag{10}$$

The critical lines are then computed by determining, on the spinodal surface, the loci where this condition is satisfied.

In binary mixtures critical end points (CEP) can be also found. These are the points where a critical phase coexists with a noncritical one. However, within TPT, the determination of the CEP requires the calculations of the whole coexisting states to assess where a critical line meet the coexisting surface related to another critical line. This was done for type II-β (section 4.3.1). Comparisons with the MSA results allow one to give a good estimate for type II-α as well (section 4.3.2). For the other mixtures, in particular for the asymmetric ones, we just indicate the approximate locations where we expect the critical end points to be present. The latter are thus denoted CEP? and the metastable part of the critical line is indicated by small (white) dots.

3. Model

The particles interact via the hard core Yukawa (HCY) pair potential $u_{ij}(r)$. The interaction between like particles is the same, ($u_{11} = u_{22}$), while unlike particles have a weaker energy of interaction, $u_{12}(r) = \delta u_{ii}(r)$, with $\delta < 1$. The HCY potential has been adopted in several studies of the symmetric mixtures based on the self-consistent Ornstein Zernicke approximation (SCOZA) [4], MSA [9] or HRT [3]. The particles are additive hard spheres and their attractive tail is given by an attractive Yukawa potential:

$$u_{ij}(r) = \begin{cases} \infty & \text{if } r \leqslant d_{ij} \\ -\epsilon_{ij} d_{ij} \mathrm{e}^{-z(r/d_{ij}-1)}/r & \text{if } r > d_{ij}. \end{cases} \tag{11}$$

The parameters ϵ_{ij} and z, define the energy scale and the range of the interactions respectively. The former is taken unitary. The inverse range of the interaction has been fixed to $z = 1.8$

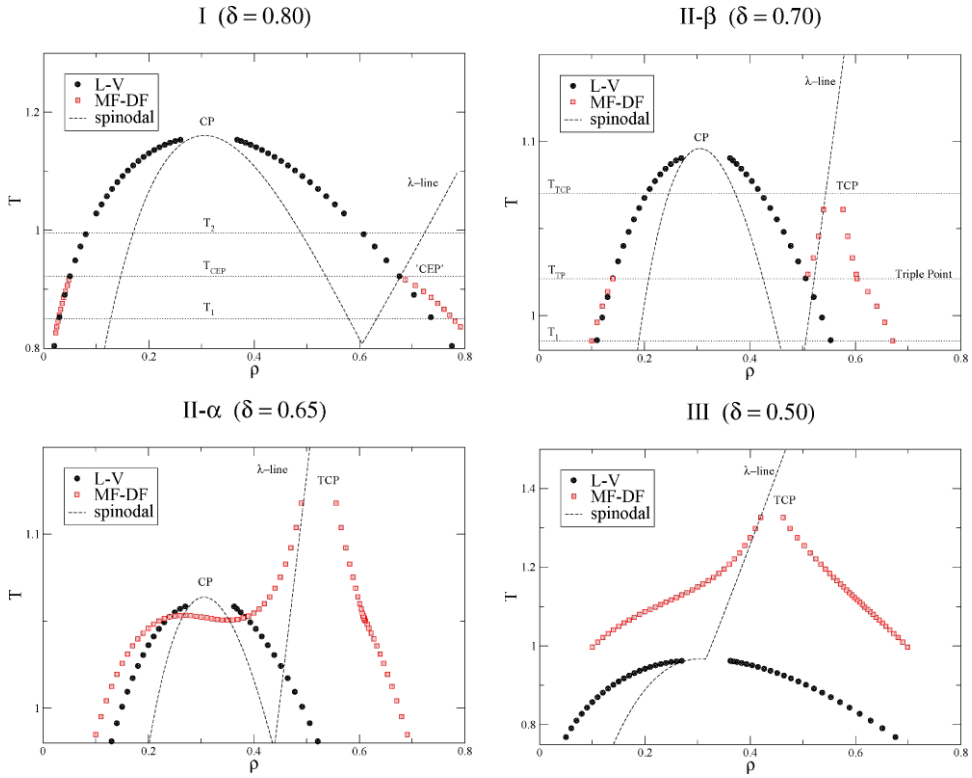

Figure 1. TPT phase diagram of the symmetric binary mixture at $x = 0.5$ representing the possible topologies of phase diagrams (I, II-α, II-β and III for $\delta = 0.8, 0.65, 0.7$ and 0.5 respectively). Beyond the λ-line, the fluid demixes into two phases of same density but with concentrations $\overline{x}$ and $1 - \overline{x}$. Depending on δ, critical points (CP), critical end points (CEP), tricritical points (TCP) and triple points (TP) can occur. The tendency for the solution to demix is enhanced when lowering δ.

for both like and unlike species. This value of the screening length has been used in the aforementioned studies on HCY symmetric binary mixtures [3, 4, 9]. Indeed, it has been shown that the HCY potential provides a reasonable description of simple fluid for $z = 1.8$, as well as colloidal suspensions, where typically $z \gg 1$. The symmetric binary mixture is composed of particles that have the same size $d_{11} = d_{22} = d_{12} = d = 1$. In a second step, mixtures of particles with size ratio $\Delta = d_2/d_1$ different from one will be considered. In that case $d_{11} = d = 1$ is kept fixed while the size of the second component is increased ($d_{22} > d$ and $d_{12} = 1/2(d + d_{22})$).

4. Phase behaviour of the symmetric binary mixtures

4.1. Phase behaviour at $x = 1/2$

The phase diagram of symmetric binary mixtures was first studied focusing on the particular plane of equal species concentration ($x = 1/2$) [4, 5]. In this simplified case, when the parameter δ varies from 0 to 1, three different topologies of phase diagrams, arising from the competition between gas and mixed-fluid (G–MF) transition and demixing transition, have been observed and classified. The mean field phase diagram at equal species concentration presents both a first-order coexistence boundary between a low density fluid and a high density one, and the so-called λ line of mixing–demixing critical points. When crossing this line, the fluid demixes into two phases of the same density but with concentrations $\overline{x}$ and $1 - \overline{x}$. Depending on the loci where the λ line crosses the G–MF transition, three types of phase diagrams have been defined (types I, II and III) [3–5]. This classification is based on the projection of the phase diagram on the $x = 1/2$ plane, and was suggested first by Tavares *et al* [23]. The calculation of the phase diagram on the whole x–ρ plane reveals the presence of two subtypes for the type II of phase diagrams [9], as will be shown.

We will present now the phase diagrams of symmetric binary mixtures we obtained from perturbation theory. In particular, we start with the description of the three different topologies of symmetric phase diagrams based on their projection on the $x = 1/2$ plane. These diagrams are presented in figure 1.

4.1.1. Type I at $x = 1/2$. The first topology corresponds to high values of δ ($\delta_1 < \delta < 1$ with $\delta_1 = 0.708$ within the mean field) and is depicted in the upper left panel of figure 1 for $\delta = 0.8$. At low temperature (T_1 on the figure) a gas at $x = 0.5$ coexists with two demixed fluids of the same density but opposite relative composition ($\overline{x}$ and $1 - \overline{x}$). Indeed, when crossing the λ line, the system separates into a component 1-rich phase and a component 2-rich phase. The coexistence between a gas and a mixed fluid (which we will call from now on a liquid–vapour LV coexistence) is also present, but metastable with respect to the previous one. At higher temperature (T_2), the gas and the homogeneous fluid

($x = 0.5$) coexist and their coexistence curve ends into a liquid–vapour critical point (CP). The λ line intersects the L–V coexistence curve well below the L–V critical point at T_{CEP}, in what appears to be a *critical end point* (CEP), i.e. a point where a critical liquid coexists with a noncritical gas. The presence of a CEP has been obtained by different authors within MF and SCOZA calculations [3, 4]. However, the determination of the critical lines on the whole ρ–x space, presented in the next sections, seems to indicate that a critical end point might not necessarily be present, in agreement with HRT and modified hypernetted chain (MHNC) calculations [3, 6].

4.1.2. Type III at $x = 1/2$. By decreasing δ, the propensity of the mixture to demix is enhanced, and the L–V coexistence curve moves to lower temperature. At small δ ($0 < \delta < \delta_2$, with $\delta_2 = 0.605$ within MF) the point at which the coexistence curve intersects the λ line coincides with its critical point. Critical point means here: the locus where the homogeneous low density gas become critical. This point is called the tricritical point (TCP): on approaching it from low temperature, the simultaneous coalescence of three phases is observed, namely a low density and homogeneous gas, and two demixed high density fluids. There is now no first-order L–V transition between the gas and the mixed fluid (the corresponding coexistence curve being metastable) and also no L–V critical point. This topology of phase diagram is shown in the lower right panel of figure 1 for $\delta = 0.5$.

4.1.3. Type II-α and II-β at $x = 1/2$. An intermediate topology (type II) is found in a narrow interval ($\delta_2 < \delta < \delta_1$). An example is presented in the upper right panel of figure 1 (subtype II-β with $\delta = 0.7$). At low temperature, T_1, an homogeneous gas coexists with two demixed fluids, as in type I. The λ line intersects the L–V coexistence just below the critical point of the L–V transition, which is also present as in type I. At T_{TP}, we observe the occurrence of a triple point where a gas, a mixed liquid at intermediate density and a 1-rich and a 2-rich liquid at high density coexist. By increasing the temperature up to T_{TCP}, the homogeneous liquid and the two demixed fluids become critical at the same tricritical point (as in type III). A second subtype (II-α) is also found for slightly lower δ, and the phase diagram is drawn on the lower left panel of figure 1 ($\delta = 0.65$). Except for the relative location of the TCP with respect to the CP, the distinction between the II-α and II-β subtypes is not possible from the $x = 1/2$ cuts[1], but the difference will become clear when considering the phase diagram on the entire x–ρ space and the connection between the different critical lines, as we will see in the next sections.

4.2. Accuracy of TPT for the symmetric binary mixture

Before moving to the determination of the phase diagram on the whole x–ρ plane we will test the accuracy of TPT in predicting the critical loci of the symmetric binary mixture.

[1] In fact, for a δ value at the boundary between cases II-α and II-β, the temperature of the tricritical point might be even higher than the minimum along the critical line CL_4 of case II-β (see figure 4), thus making impossible the distinction between the two subtypes from the $x = 1/2$ cuts alone.

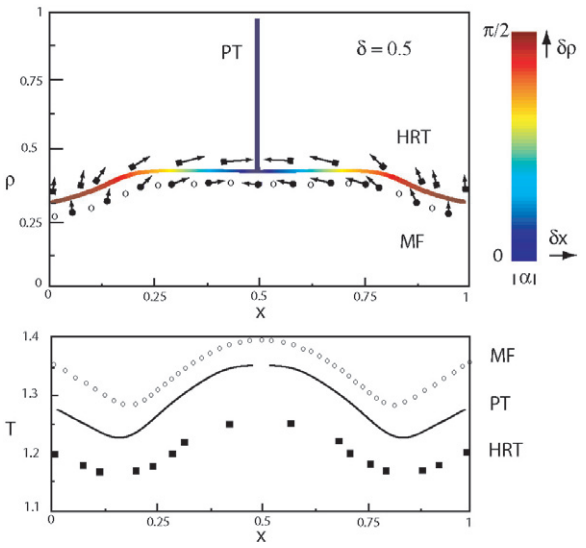

Figure 2. Projection of the critical lines in the x–ρ plane (upper panel) and x–T plane (lower panel) for $\delta = 0.5$ as obtained from perturbation theory, HRT and MF calculations (from [3]). The TPT critical lines lie in between MF and the more accurate HRT results in both projections. The stability indicator, α, is also drawn on the TPT critical line ($0 < |\alpha| < \pi/2$). For $\alpha = 0$ (horizontal arrow), fluctuations in concentration x drive the phase separation and demixing is found, as observed at $x = 1/2$. When $|\alpha| = \pi/2$ (vertical arrow), the system becomes critical because of density fluctuations and the L–V transition occurs, as found in the one component limits ($x = 0$ and 1).

Figure 2 shows the projections of the HRT, MF and TPT critical lines on both the ρ–x and the x–T planes for the type III phase diagram ($\delta = 0.5$). This value of δ is small enough to give the same topologies of the critical lines in HRT, mean field theory and also TPT. The TPT critical lines are found to fall in between the results of HRT and MF. For the pure species, it is known, from the comparison with accurate simulation data for the critical point of the Yukawa fluid with the same $z = 1.8$ inverse range considered here [24], that TPT underestimates by about 10% the critical density and overestimates by about 5% the critical temperature. It has been shown that HRT provides a very good determination of the critical point for Lennard-Jones like fluids [25] and we found for the critical loci of the binary system the same differences between TPT and the accurate HRT, as for the pure fluid case.

The relatively long range of the attraction ($z = 1.8$) is responsible, at least in part, for this accuracy: it is well known that the error within TPT on the location of the critical density for one component systems becomes smaller and smaller when the range of the potential increases [26]. But our results provide an evident improvement with respect to other mean field theories and TPT is certainly a valuable method to study the phase behaviour of binary mixtures.

The stability indicator, α, defined above, which indicates the kind of fluctuations that are driving the phase separation process, is also drawn on the critical line in figure 2. For the pure one component solutions, fluctuations in density ($|\alpha| = \pi/2$, red) lead to L–V phase separation, while at $x = 1/2$, along the λ-line, pure fluctuations in concentration ($\alpha = 0$,

blue) are responsible for the demixing of the solution. The value of α, which gives the direction of the order parameter of the transition, will also be drawn in the next figures on the different critical lines, using the same definition for the colours associated with the possible values of α as presented in figure 2.

4.3. Phase behaviour in the x–ρ plane

We will describe now the phase behaviour of symmetric binary mixtures on the whole x–ρ plane. The critical lines and the phase behaviour of the different type of phase diagrams that were defined in the preceding section will be determined. We start the investigation by a careful study of subtype II, thus focusing on the set of interparticle strengths for which the phase diagram at equal concentration exhibits both a liquid–vapour critical point and a tricritical point. MSA results for this topology of phase diagrams showed two possible subtypes [9]. Following the definitions introduced before, we present now a detailed study of subtype II-β. The other phase diagrams will be then also presented, but more briefly.

4.3.1. Phase diagram of type II-β. The phase diagram of type II-β is depicted in figure 3. Four critical lines CL_i can be distinguished. Each critical line spans along a well defined coexistence surface S_i. CL_1 is the λ line, the critical line of the symmetrical demixing surface S_1 present at high density. At the tricritical point, CL_1 bifurcates and gives rise to two critical lines, CL_2 and CL_3, that cross the surfaces S_2 and S_3 (composed of the green small dots). These critical lines terminate in critical end points (CEP) when reaching the fourth coexistence surface S_4 which spans along the whole concentration range. CL_4, the critical line related to S_4, connects the pure component liquid–vapour critical points and is totally disconnected from the λ line. Some other aspects of the phase behaviour of the subtype II-β (cuts of the spinodal surface at different temperature and the stability indicator on the critical line) are also depicted in the upper right panel of figure 4.

The critical lines presented on figure 3 were obtained solving equation (10) on the instability surface. Using this efficient method to compute the critical lines, we found peculiar critical loops at intermediate concentration and density, made of CL_2, CL_3 and of two low density branches (L_2 and L_3). In a second step, the coexistence surfaces were determined and, from the extrapolation of the coexistence points, we verified the location of the critical lines previously calculated. In this way, we found that CL_2 and CL_3 end in CEP, while L_2 and L_3 are located below the coexistence surface S_4 and, thus, are metastable. We note a very good correspondence between these lines and the location in the x–ρ plane of two *triple lines* in MSA calculations [9]. These triple lines were defined by the intersection of coexisting surfaces (in this case where S_4 intersects S_2 and S_3). The triple lines are not critical lines, but they are located on the binodal surface. The close similarity we found between L_2, L_3 and the triple lines of [9] could be due to S_4 and S_3 (or S_4 and S_2) meeting very close to (but not exactly at) the stability boundary of either of them.

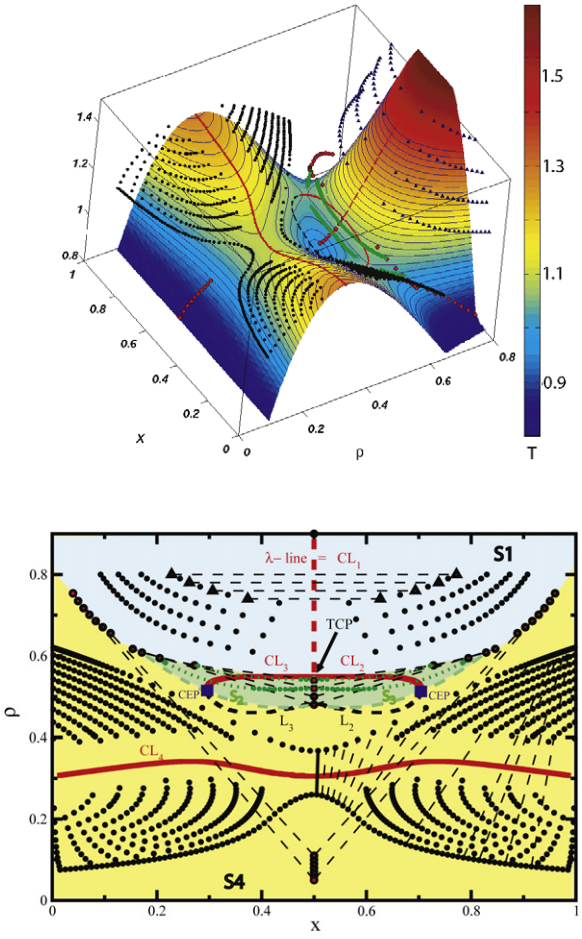

Figure 3. TPT phase diagram of the $\delta = 0.7$ symmetric binary mixture (upper panel) and its projection onto the x–ρ plane (lower panel). The underlying spinodal surface is coloured in the 3D diagram. The critical lines (CL_i) are drawn in red. In order to obtain the four coexistence surfaces S_i (coloured in the lower panel), we calculated coexisting states (dark dots). Up to three coexisting states were found. Some tie lines joining the coexisting phases are drawn (dashed thin lines). The green dots (and green line) are coexisting phases that join at CL_2 and CL_3, and the critical end points (CEP) of CL_2 and CL_3 are also drawn (blue squares). The dashed red line is the mixing–demixing λ line (CL_1), with some of the corresponding coexisting states depicted by triangles. The dashed lines (L_2 and L_3) are solutions of equation (10) but located below the coexistence surface. The large red dots represent the triple line.

4.3.2. Phase behaviour of the remaining type (II-α, I and III). A second subtype of phase diagram II has been also defined and is depicted in the lower left panel of figure 4 for $\delta = 0.65$: for this subtype II-α, the λ line bifurcates at the tricritical point into two critical lines which pass through minima and connect to the liquid–vapour critical points of the pure phases. This, indeed, is in contrast with subtype β, where CL_4, the critical line arising from the pure component critical points, is totally disconnected from the λ line, and this leads to the distinction between the two subtypes. Within TPT the transition between the two topologies is found around $\delta = 0.6694$.

A peculiar solution for the loci of critical points is obtained for subtype α as well. In that case, a loop of points, the solution of equation (10), is found around $x = 0.5$, but,

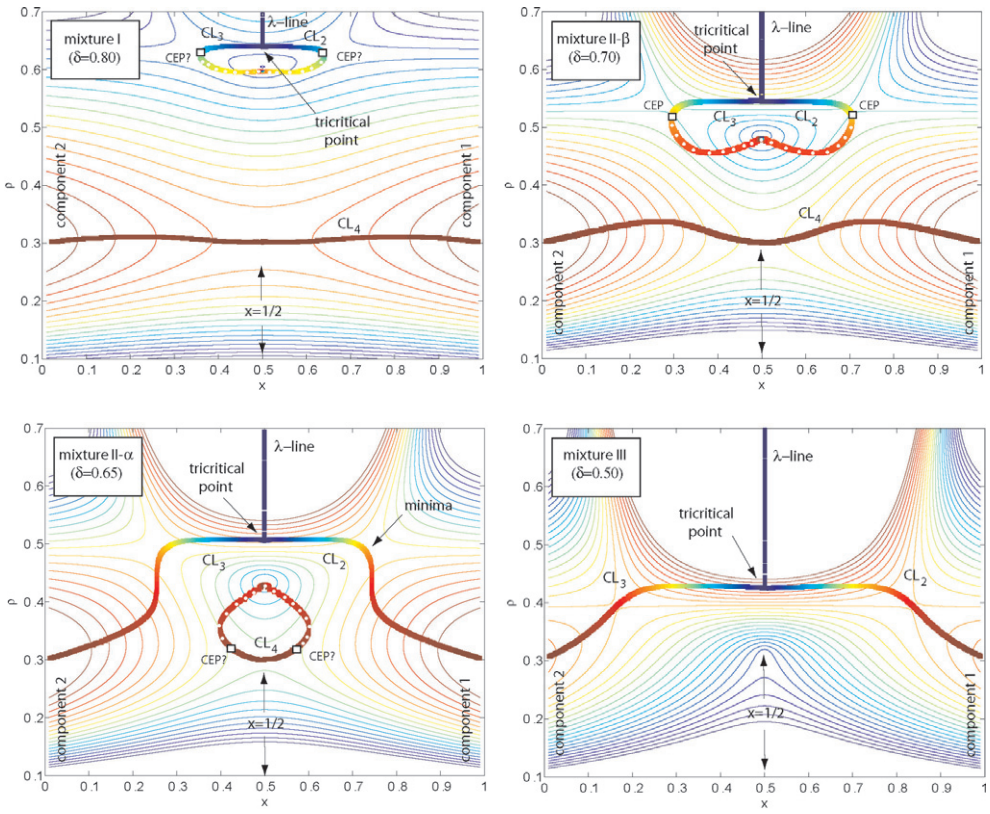

Figure 4. The four different types of phase diagrams for the symmetric binary mixture are depicted ($\delta = 0.8, 0.7, 0.65, 0.5$). The projection of the critical lines onto the x–ρ plane and cuts of the instability surface for different temperatures (0.8–1.24 by steps of 0.02) are shown. The transition between the two subtypes of topology II ($\delta = 0.70$ and 0.65) is found around $\delta = 0.6694$. The critical end points are represented by small squares. The value of the stability indicator α on the critical lines is also shown (according to the scale introduced on figure 2). The dotted lines denote metastable parts of the critical lines.

from the analysis of the coexistence points, only the lower part corresponds to a critical line, in agreement with the MSA study [9]. Thus, the determination of the spinodal and the critical loci from equation (10) is certainly a very efficient tool to map the topology of the phase diagram but it should be complemented by the computationally more involved determination of the coexisting points. The necessity of also computing the set of coexisting points and tie lines will become crucial when dealing with more complex binary mixtures [14].

Phase behaviours corresponding to the remaining topologies (type I and III) are also depicted in figure 4. Interestingly, from the calculations of the critical lines for the $\delta = 0.8$ case, it seems that the λ-line does not end in a CEP at $x = 1/2$, contrary to what the analysis at $x = 1/2$ tends to show. The mixture seems still to be in the intermediate regime (II-β), with the occurrence of a tricritical point and the presence of very tiny coexistence surfaces (S_2 and S_3) and their connected critical lines. We do not observe the clear occurrence of a CEP at $x = 1/2$ up to $\delta = 0.9$, the central loops made of CL_2, L_2 and CL_3, L_3 becoming just narrower. For higher δ, the intermediate coexistence surfaces become so small that their presence is very difficult to assess. However, in order to assess if, indeed, a tricritical point persists up to high values of δ, the stability of the critical lines CL_2 and CL_3 with respect to the first-order phase transition should be carefully investigated and the whole coexistence boundaries computed. An absence of CEP would be in qualitative agreement with studies based on HRT and MHNC which did not find any critical end point at equimolar species up to $\delta = 0.8$ [3, 6]. At the same time, simulations performed on square well potentials found the CEP characteristic of topology I already at around $\delta = 0.7$ [5] and the same behaviour was observed in Monte Carlo simulation of Lennard-Jones symmetric mixtures [27].

The important conclusion we can draw at this point, is that the phase diagrams of the binary symmetric mixtures are well reproduced by perturbation theory and we can rely on it to investigate the phase diagrams of more realistic mixtures. As a first step in this direction, we will study now what is the effect, on the phase diagram, of introducing an asymmetry $\Delta = d_2/d_1$ into the binary mixtures.

5. Phase behaviour of asymmetric binary mixtures ($d_1 \neq d_2$)

In this section, we present an overview of the phase behaviour of the different phase diagram topologies presented above when introducing a slight asymmetry in the diameter of the two components. The spinodal instability and the critical lines are determined for the different mixtures and give a first insight

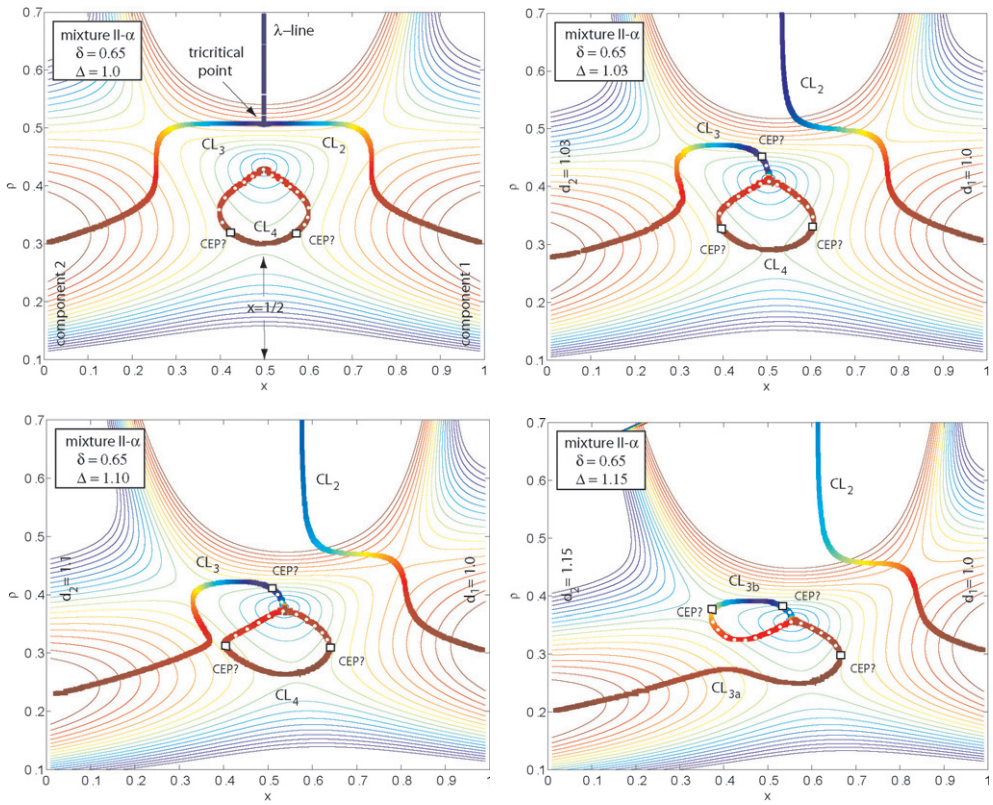

Figure 5. Phase behaviour of type II-α phase diagram ($\delta = 0.65$) of the symmetric mixture for different $\Delta = d_2/d_1$ ratios. The projection of the critical lines onto the x–ρ plane and cuts of the instability surface for different temperatures (0.8–1.24 by steps of 0.02) are shown for $\Delta = 1, 1.03, 1.1, 1.15$, as indicated on the panels. The λ-line of the demixing transition is connected to the LV critical point of the pure small component ($x = 1$) for $\Delta > 1$. The squares are estimates of the critical end points CEP locations and the dotted lines denote metastable parts of the critical lines.

into their phase diagram. This study might be complemented by a more careful determination of the coexistence surfaces which will also assess the exact location of the critical lines and critical end points. However, for the scope of the present study, the determination of the spinodal and the calculations of the critical lines through equation (10) will already give important insights into the effect of size asymmetry on the phase diagram. The complete determination through TPT of the phase diagram of a more specific binary mixture, namely a model for solution of α and γ eye lens proteins, can be found in [14].

We consider the same HCY interaction between the two components (equation (11)) as for the symmetric case. The inverse screening length is kept fixed ($z = 1.8$) and we only increase the diameter of the second component d_2. In this way, the effective range of interaction between the components of kind 2 is reduced, and the critical point of the pure mixture of component 2 should move correspondingly to lower T and higher ϕ when increasing Δ. However, for the HCY with $z = 1.8$ the change in the range of the second component is almost negligible. For the highest ratio $\Delta = 1.25$ considered in this study, the location of the critical point changes by less than 0.2% with respect to $\Delta = 1$. Thus, changes to the phase behaviour of the binary mixtures observed when increasing Δ are caused essentially by the size asymmetry and not by the change in the interactions between the components.

5.1. Phase behaviour of type II-α

For subtype II-α, two interesting features appear when Δ increases and the symmetry with respect to $x = 1/2$ is broken (figure 5). First, the λ line of the demixing transition is connected to the liquid vapour critical point of the pure solution of the smallest component only, as soon as $d_1 \neq d_2$, forming a single critical line denoted by CL_2 on the panels with $\Delta \neq 1$. Along this critical line, the fluctuations responsible for the phase separations change from density–density fluctuations near $x = 0$, to essentially concentration–concentration fluctuations near $x = 0.5$.

We expect the critical line CL_3 of the second and bigger component to end in a critical end point at intermediate density and composition, near the locus where the λ line bifurcates into CL_2 and CL_3 at $\Delta = 1$. The exact location of this end point has not been determined, as explained above, but the expected location is indicated (CEP? symbol).

Second, as d_2 increases further, the critical line CL_3 arising from the critical point of the pure large component extends towards lower densities and, at around $\Delta = 1.15$, detaches from its intermediate density branch (CL_{3b}) to join the critical line that comes from the liquid vapour critical point at $x = 1/2$, and that was already present in the case of the symmetric mixture. This gives rise to a new critical line CL_{3a}, as shown on the lower right panel. The small coexistence

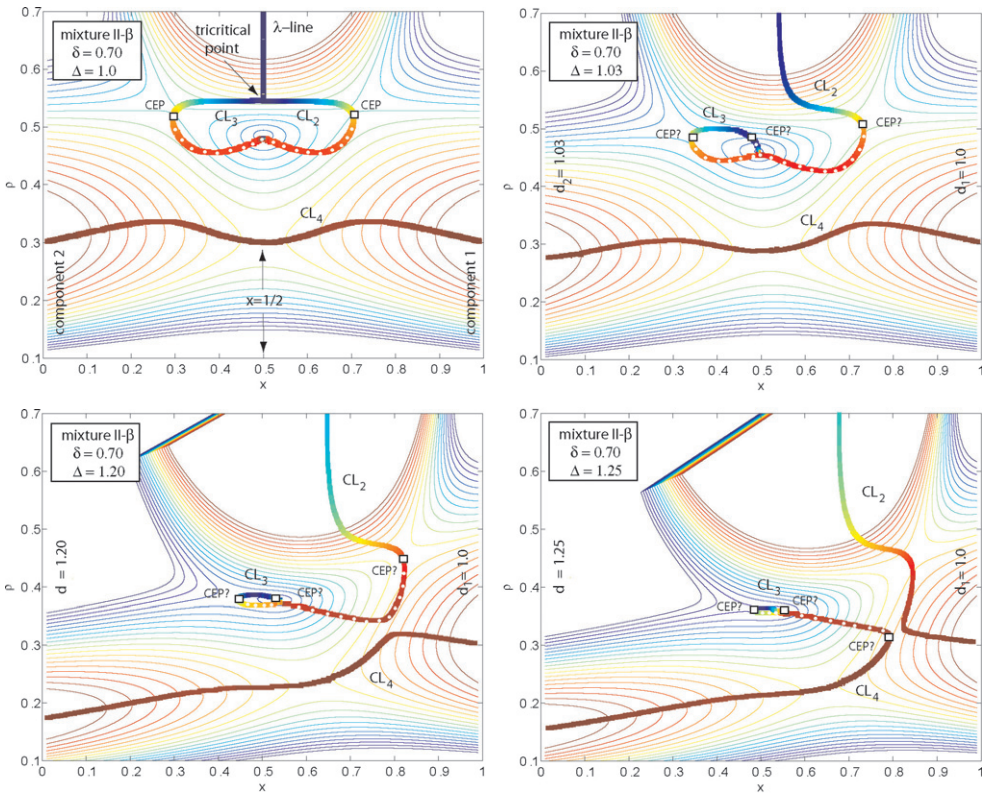

Figure 6. Phase behaviour of type II-β phase diagram ($\delta = 0.7$) of the symmetric mixture for different $\Delta = d_2/d_1$ ratios. The projection of the critical lines onto the x–ρ plane and cuts of the instability surface for different temperatures (0.8–1.24 by steps of 0.02) are shown for $\Delta = 1, 1.03, 1.2, 1.25$, as indicated on the panels. The squares show the critical end points (CEP) and the dotted lines denote metastable parts of the critical lines. For $\Delta = 1.25$, the λ line connects the LV critical point of the pure small component ($x = 1$).

surface around CL_{3b} is still present at $\Delta = 1.15$ but will disappear at larger asymmetry.

5.2. Phase behaviour of type II-β

The phase behaviours for subtype II-β are depicted in figure 6. For $\Delta \neq 1$, the λ line detaches from the critical line CL_3 that crosses the coexistence surface S3 for the symmetric mixture (as defined on figure 3) and connects to CL_2 only. This critical line, called now CL_2, moves when increasing Δ towards lower densities and larger x (i.e. towards the pure mixture of small components), coming closer and closer to CL_4, which exhibits a strong bending (see the kink around $(x, \rho) = (0.8, 0.3)$ in the $\Delta = 1.20$ panel). Moreover, we expect the detached CL_3 now to have two critical end points (CEP?).

At $\Delta = 1.25$, the critical point of the pure small component finally connects to CL_2, CL_2 expanding now from the former λ line present at $\Delta = 1$ to the pure mixture of component 1 ($x = 1$), as is found in the II-α subtype for $\Delta > 1$. The critical line CL_3 is still present but will disappear for larger Δ.

5.3. Phase behaviour of type I and III

The phase behaviours for $\delta = 0.8$ are presented in the upper panels of figure 7. We observe qualitatively the same phase behaviour as for type II-β, with the λ line that we speculate to be connected to the small component critical point at higher Δ. Thus, also for the asymmetric case, no type I topology seems to be found within TPT.

The phase behaviour of type III is less rich and interesting than the previous ones (see lower panels of figure 7). The critical point of the pure solution of large particles is totally disconnected from the λ line as soon as $\Delta > 1$, and a critical end point is expected. The λ line connects to the LV critical points of the pure solution of small components (CL_2 on the lower left panel).

In conclusion, we observed that for sufficiently large asymmetry (the value of Δ required depends on δ) the λ-line is always connected to the critical point of the smallest component only. Because of the attractive interaction between the particles, the system is expected to undergo a liquid–vapour transition for suitable x, ρ and T. This happens already in the symmetric case at low or high concentration x, where one of the components does not influence the L–V transition of the other species. Moreover, since $\delta < 1$ (i.e. $\epsilon_{ij} < \epsilon_{ii}$), the internal energy tends to promote demixing between the two components. At sufficiently high density, the loss of entropy induced by demixing might be overcome by the increase in the absolute value of the internal energy. In this case, the system undergoes a mixing–demixing transition, as we observed in all symmetric mixtures investigated.

In the case of $\Delta > 1$, the propensity for the mixture to demix while increasing the concentration of the largest

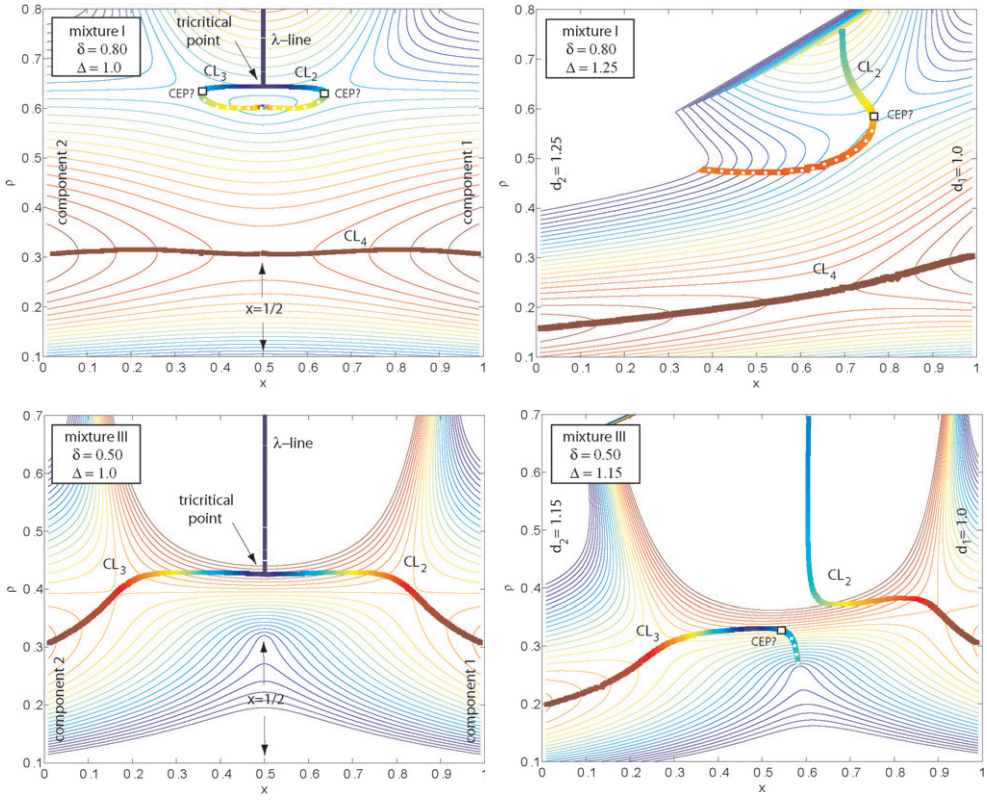

Figure 7. Phase behaviour of type III ($\epsilon_{ij} = 0.5$) is depicted in the lower panels for $\Delta = 1, 1.15$ (left and right respectively). The $\epsilon_{ij} = 0.8$ case is shown in the upper panels ($\Delta = 1, 1.25$, left and right respectively). The projection of the critical lines onto the x–ρ plane and cuts of the instability surface for different temperatures (0.6–1.6 by step of 0.03 for $\epsilon_{12} = 0.8$ and 0.88–1.24 by steps of 0.02 for type III) are drawn.

component becomes stronger and stronger with increasing asymmetry, for all values of δ. Indeed, from the same argument we just mentioned, it is clear that when $d_2 > d_1$ and $\epsilon_{12} < \epsilon_{ii}$, the loss in internal energy when adding some components-2 to a solution of components-1 is more important than for the equal size case, since more energetically favourable 1–1 contacts are lost. The loss of entropy resulting from the demixing of the solution is then overcome at much smaller density. Thus, the tendency of the mixture to demix is enhanced and the corresponding critical line moves to higher concentrations x and lower densities.

In contrast, the mixing–demixing transition is less favoured in a solution made principally of the large components (at small x) when adding small components, and the critical point of the larger component is always disconnected from the λ-line at high Δ. The situation might change for large Δ ($\Delta \sim 5$), when depletion induced interactions between the largest components might also appear [28, 29].

6. Conclusions

In this paper we used thermodynamic perturbation theory to study the phase behaviour of symmetric binary mixtures interacting via a hard core Yukawa potential. We showed that TPT is not only suited for describing the phase diagram of one component system, but it also accounts well for the phase diagram of binary mixtures. The main topologies of the symmetric binary mixtures phase diagram were correctly reproduced within TPT, in agreement with advanced liquid state theories, such as HRT. We also discussed the qualitative and predictive capacity of TPT and demonstrated that this method provides a clear improvement with respect to standard mean field approaches.

As a first step towards nonsymmetric mixtures, we showed in the last section that perturbation theory can be straightforwardly extended to mixtures that are not symmetric in size. Interestingly, when the energy of interaction between unlike particles is weaker than the interaction between like particles ($\delta < 1$), the propensity for a solution of two components to demix becomes stronger when the asymmetry $\Delta = d_1/d_2$ increases. Indeed, for sufficiently large asymmetry (the value of Δ required depends on δ) the λ-line always connects the critical point of the smallest component and never the critical line of the large component.

Acknowledgments

We thank G Kahl and D Pini for useful discussion and suggestions. ND thanks especially G Kahl for hospitality. ND and GF acknowledge the support of the Swiss National Science Foundation (Grant No. 200021-105382/1 and PP0022 119006). The support of CECAM during the workshops 'Computer Simulation Approaches to Study Self-Assembly: from Patchy Nano-Colloids to Virus Capsids' and 'New Trends

in Simulating Colloids: From Models to Applications' is also acknowledged.

References

[1] Hansen J P and McDonald I R 1986 *Theory of Simple Liquids* 2nd edn (London: Academic)
[2] Swinton F L and Rowlinson J S 1982 *Liquids and Liquid Mixtures* 3rd edn (London: Butterworths)
[3] Pini D, Tau M, Parola A and Reatto L 2003 *Phys. Rev.* E **67** 046116
[4] Scholl-Paschinger E and Kahl G 2003 *J. Chem. Phys.* **118** 7414
[5] Wilding N B, Schmid F and Nielaba P 1998 *Phys. Rev.* E **58** 2201
[6] Antonevych O, Forstmann F and Diaz-Herrera E 2002 *Phys. Rev.* E **65** 061504
[7] Parola A and Reatto L 1985 *Phys. Rev.* A **31** 3309
[8] Parola A and Reatto L 1991 *Phys. Rev.* A **44** 6600
[9] Köfinger J, Wilding N B and Kahl G 2006 *J. Chem. Phys.* **125** 234503
[10] Pini D, Parola A and Reatto L 2000 *J. Stat. Phys.* **100** 13
[11] Gast A P, Russell W B and Hall C K 1983 *J. Colloid Interface Sci.* **96** 251
[12] Foffi G, McCullagh G D, Lawlor A, Zaccarelli E, Dawson K A, Sciortino F, Tartaglia P, Pini D and Stell G 2002 *Phys. Rev.* E **65** 031407
[13] Stradner A, Foffi G, Dorsaz N, Thurston G M and Schurtenberger P 2007 *Phys. Rev. Lett.* **99** 198103
[14] Dorsaz N, Thurston G M, Stradner A, Schurtenberger P and Foffi G 2009 *J. Phys. Chem.* B **113** 1693
[15] Barker J A and Henderson D 1967 *J. Chem. Phys.* **47** 2856
[16] Mansoori G A, Carnahan N F, Starling K E and Leland T W 1971 *J. Chem. Phys.* **54** 1523
[17] Lebowitz J L 1964 *Phys. Rev.* **133** A895
[18] Verlet L and Weis J 1972 *Phys. Rev.* A **5** 939
[19] Grundke E W and Henderson D 1972 *Mol. Phys.* **24** 269
[20] Tisza L 1966 *Generalized Thermodynamics* (Cambridge, MA: MIT Press)
[21] Chen X S and Forstmann F 1992 *J. Chem. Phys.* **97** 3696
[22] Bhatia A B and Thornton D E 1970 *Phys. Rev.* B **2** 3004
[23] Tavares J M, Telo da Gama M M, Teixeira P I C, Weis J J and Nijmeijer M J P 1995 *Phys. Rev.* E **52** 1915
[24] Pini D, Stell G and Wilding N B 1998 *Mol. Phys.* **95** 483
[25] Parola A and Reatto L 1995 *Adv. Phys.* **44** 211
[26] Vega L, de Miguel E and Rull L F 1992 *J. Chem. Phys.* **96** 2296
[27] Wilding N B 2003 *Phys. Rev.* E **67** 052503
[28] Biben T and Hansen J P 1991 *Phys. Rev. Lett.* **66** 2215
[29] Louis A A 2001 *Phil. Trans. R. Soc.* A **359** 939